RP Current Trends In Engineering And Technology
Vol. 3, No. 2 (April – June 2024) pp. 34–39
e-ISSN: 2583-5491

RESEARCH PLATEAU PUBLISHERS

Cite this article: G. Kumar, R. Kumar, R.S. Bharj, Efficient cooling system for lithium-ion battery pack by using non-Newtonian nano fluid in cooling channel under laminar flow: A numerical analysis, *RP Cur. Tr. Eng. Tech.* **3** (2024) 34–39.

Original Research Article

Efficient cooling system for lithium-ion battery pack by using non-Newtonian nano-fluid in cooling channel under laminar flow: A numerical analysis

Gajendra Kumar*, Rajan Kumar, Rabinder Singh Bharj
Dr. B.R. Ambedkar National Institute of Technology, Jalandhar, Punjab 144008, India
*Corresponding author, E-mail: gajendrak.te.22@nitj.ac.in

ARTICLE HISTORY
Received: 31 July 2024
Revised: 14 August 2024
Accepted: 16 August 2024
Published online: 19 August 2024

KEYWORDS
Lithium-ion battery;
Cooling channel;
Nano-fluid;
Cooling performance;
Numerical analysis.

ABSTRACT
To enhance the efficiency and prolong the lifespan of the power battery module in electric vehicles, we propose a Battery Thermal Management System (BTMS) that incorporates liquid cooling. This study focuses on a numerical investigation aimed at assessing the effectiveness of a cooling channel in reducing thermal non-uniformity in the performance of lithium-ion battery packs. A specially designed wrapped cooling channel is employed to augment the heat transfer area, and its cooling performance under liquid cooling is examined. The chosen liquid coolant is a nano-fluid consisting of multi-wall carbon nanotubes (MWCNT) as nano-particles, mixed with a base fluid of distilled water and ethylene glycol. The analysis considers various parameters, including mass flow rate, discharge rate, and configuration, to evaluate cooling performance. The numerical solution employs the laminar flow regime and the SIMPLE method. The results indicate superior cooling performance achieved by the proposed wrapped cooling channel. This approach demonstrates promising results for mitigating thermal non-uniformities and improving the overall performance of lithium-ion battery packs in electric vehicles.

1. Introduction

Addressing climate change is a pressing global challenge, primarily driven by the rise in carbon dioxide levels, largely from industrial and transportation activities. Transportation, particularly through internal combustion engines, significantly contributes to CO_2 emissions, totaling 7.3 billion metric tons in 2020. To mitigate air pollution and noise, there is a growing shift towards electric vehicles (EVs), which produce minimal to zero emissions compared to traditional vehicles [1]. EVs rely on Lithium-ion battery packs for power due to their high energy density and voltage capacity. These packs consist of numerous cells arranged in series and parallel configurations. The performance, lifespan and safety, of these cells depend heavily on their operating temperature, ideally between 20°C to 40°C. Maintaining this temperature range is critical during charging and discharging processes to ensure optimal performance and safety. To manage heat generated during these processes, Battery Thermal Management Systems (BTMS) are essential. Figure 1 illustrates a visual representation of battery issues due to heat accumulations, indicating that if the heat generated during discharging and charging lower than dissipation, the battery remains in a safe zone. However, if heat generation surpasses dissipation, proper battery thermal management becomes imperative. In the presence of thermal runaway, mechanical, electrical, and thermal stresses issue, subsequently leading to overheating, combustion, explosion, and the release of gases [2]. There are mainly three BTMS systems are widely used to thermal management of battery packs. Liquid cooling, air cooling and phase change material. One another BTMS is also commonly come in senior that is hybrid BTMS, in this hybrid system adopted any two parallel as thermal management [3-4]. At present, liquid cooling continues to be the predominant method for BTMS. Exploring the avenue of upgrading the standard cooling medium to one with higher thermal conductivity stands as a crucial research path to augment the efficiency of cooling systems for Lithium-ion Battery (LiB) cells. Conversely, various researchers have demonstrated the advantages of employing nano-fluids in diverse applications [5].

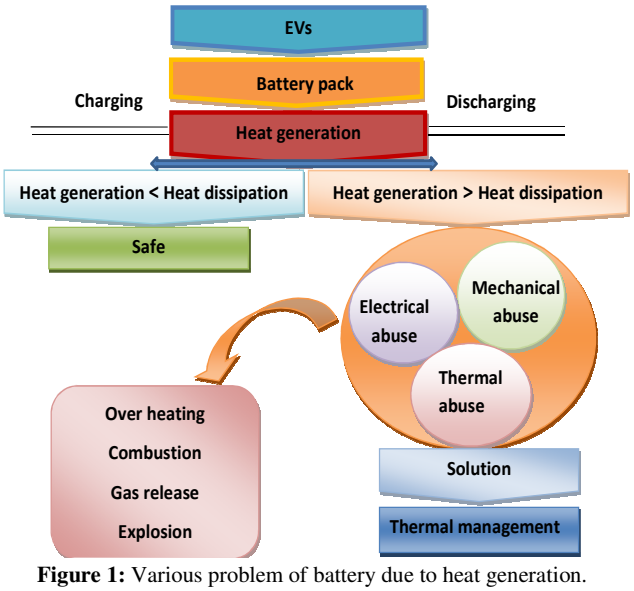

Figure 1: Various problem of battery due to heat generation.

Wiriyasart et al. [6] introduced a computational analytical technique to quantify the temperature profile and pressure loss in the corrugated mini-channel (Symmetry 2023, 15, 640) of the Electric Vehicle (EV) battery cooling unit utilizing nanofluids. The study unveiled that the type of coolant, mass flow rate, and coolant flow direction significantly influenced temperature distributions. Mokashi et al. [7] investigated the cooling capabilities of one-battery and five-battery systems. Simulation findings demonstrated that temperature maintenance was achievable using a nanofluid-based BTMS.

In this research, a liquid cooling channel is developed to enhance the thermal uniformity performance of a lithium battery pack. The design of this channel is based on the fundamental Newton law of cooling, which states that heat dissipation increases with the heat transfer area (surface contact) Therefore, the channel is designed to maximize the surface contact area with the battery cell. For comparison purposes, three additional BTMS systems are developed. BTMS 1 and BTMS 2 are the same, with only the configuration being different. Similarly, BTMS 3 and BTMS 4 are the same, with only the configuration being different. BTMS 1 and BTMS 3 have a longitudinal flow configuration, while BTMS 2 and BTMS 4 have a transverse flow configuration. Enhance the cooling performance, BTMS is investigated under various flow velocities, different nano-fluids, and different discharge rates through numerical analysis using fluent software.

2. Materials and methodology

2.1 Nano-fluids and their properties

The unique properties of nanofluids, such as enhanced thermal conductivity and heat transfer capabilities, make them interesting for various applications, particularly in heat transfer and cooling systems. The small size of the nanoparticles allows for better dispersion in the fluid, leading to improved heat transfer efficiency compared to traditional fluids. As a result, nanofluids have been explored for use in applications such as heat exchangers, electronic cooling, and even in some medical applications. It's important to note that the properties of nanofluids can be influenced by factors such as the type of nanoparticles used, their concentration, and the base fluid. Research in this field is ongoing, and scientists continue to explore new ways to optimize and utilize nanofluids for various practical applications [8].

The accurate modeling and numerical investigation of heat transfer and fluid flow in nanofluids hinge on a thorough characterization of their main thermophysical and transport properties, including density (ρ), specific heat (C_p), thermal conductivity (k), and dynamic viscosity (μ). This particular nanofluid selection relies on experimental data from 60 MWCNTs nanofluid samples, which were prepared and tested by Abreu et al. [9]. The nanofluid samples were composed of two aqueous fluids of EG at volume fractions of 30% and 60% as base fluids, incorporating six aspect ratios of the geometry distribution of MWCNTs particles.

For the upcoming investigations on heat transfer and fluid flow, each group will be denoted by a specific nanofluid (NF1, NF2, NF3, and NF4), representing the averaged properties of the respective four groups in the database.

Table 1: Lables used for each nanofluid in the following study [13].

Labels	NF1	NF2	NF3	NF4
MWCNTs Vol%	0.25	1.5	0.25	1.5
Base fluid	30%EG	30%EG	60%EG	60%EG

Table 1 provides a summary of the specific conditions that these four nanofluid groups characterize. To establish reliable thermal conductivity correlations with respect to temperature (T), polynomial fitting curves were applied to the experimental data of thermal conductivity from MWCNTs nanofluids and base fluids [10], maximum deviation of 0.5% was observed. The parameters for these correlations are outlined in Table 2.

Table 2: Non-Newtonian viscosity correlations [13].

$$K = aT^3 + bT^2 + cT^1 + d$$

Parameters	a	b	c	d
NF1	7.396E-07	-6.664E-04	2.010E-01	-1.982E+01
NF2	3.333E-07	-2.817E-04	7.987E-02	-7.105E+00
NF3	1.528E-07	-1.417E-04	4.406E-02	-4.236E+00
NF4	1.667E-07	-1.544E-04	4.797E-02	-4.605E+00

Moreover, new viscosity correlations were developed by applying a power-law fitting curve Eq. (1), to the viscosity experimental data [9]. This approach takes into account the observed non-Newtonian shear-thinning rheological behavior of MWCNTs nanofluid.

$$\mu = K\,\gamma^{n-1}\exp\left[\alpha\left(\frac{1}{T-T_0}-\frac{1}{T_\alpha-T_0}\right)\right] \quad (1)$$

In the given context, μ represents viscosity (measured in Pas), and The input parameters include K, n, α, T_0, and T_α. K serves as a metric for the average viscosity of the nanofluid, acting as the consistency index. The parameter n gauges the deviation of the fluid from Newtonian behavior, functioning as the power-law index; a value of n less than 1 indicates shear-thinning behavior. α represents the ratio of the activation energy (measured in J/K.mol) to the thermodynamic constant R (measured in J/mol.K). Additionally, T_α denotes the reference temperature (T_α =293.15 K), and T_0 represents the temperature shift (T_0 = 273 K). γ corresponds to the shear rate, measured in 1/s. the data for find viscosity is given Table 3.

Table 3: Thermal conductivity correlations [13].

	n	K	α	T_α
NF1	0.985	2.59E-03	2100	293.15
NF2	0.911	9.460E-03	2200	293.15
NF3	0.957	7.548E-03	2950	293.15
NF4	0.935	1.550E-02	2800	293.15

2.2 Methodology

2.2.1 Designed model and configuration

This research paper involves the utilization of 30 cylindrical lithium-ion cells of the 18650 type. These cells are organized in a grid pattern of 3 rows and 10 columns with a 5 mm separation between each cell; each cell has a diameter of 18 mm and a length of 65 mm. The voltage of an individual cell is 3.2 V, and its capacity is 1.35 Ah. To facilitate the circulation of coolant in the battery pack, a channel with a thickness of 3 mm and a width of 65 mm was designed. The

cooling channel wall has a thickness of 1 mm and is made of aluminum material.

Table 4: Thermo physical properties of the materials [12].

Material	ρ (Kg/m^3)	C (J/KgK)	k (W/mK)	μ (Kg/ms)
Aluminium	2719	871	202.4	-
Water	998.2	4128	0.6	1.003×10^{-3}
Battery	2018	1282	2.7	-

Table 4 shows the term physical properties of BTMs, the objective in designing the channel is to maximize the contact surface area, ensuring optimal heat dissipation. Figure 2(a) illustrates BTMS1 with the maximum contact surface area in a longitudinal flow configuration, while Figure 2(b) shows BTMS2 with maximum contact surface area in a transverse flow configuration. For comparison with the designed channels, another tangent surface contact channel is considered, as depicted in Figure 2(c) and Figure 2(d). In Figure 2(c), BTMS3 represents a longitudinal flow, and in Figure 2(d), BTMS4 represents a transverse flow.

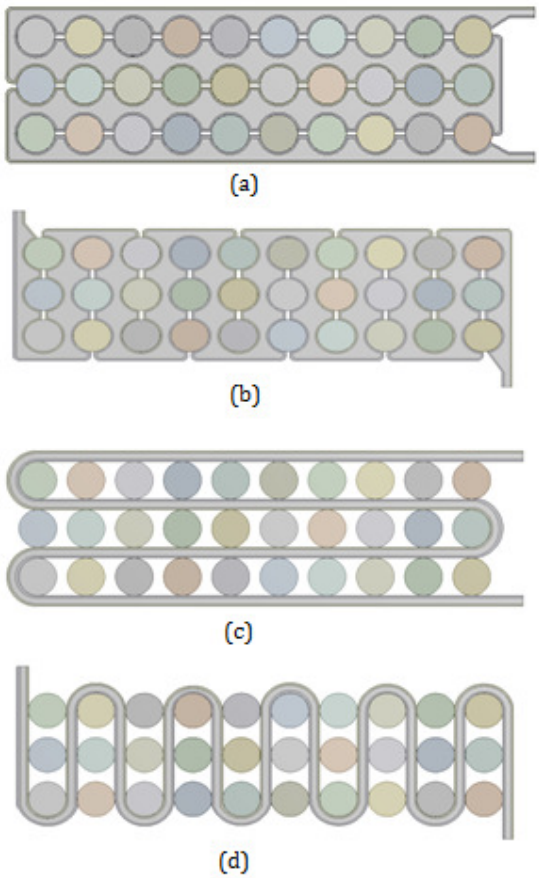

Figure 2: Various designed cooling channel, (a) BTMS1; (b) BTMS2; (C) BTMS3; (D) BTMS4.

Overall, this research comprises four BTMS systems featuring innovatively designed channels. One includes a wrapped channel, as illustrated in Figure 2 (a, b), while the other employs a simple tangent channel, shown in Figure 2 (c, d). To assess cooling performance, two configurations are considered: one in the longitudinal direction and the other in the transverse direction with respect to the battery pack. A non-Newtonian MWCNTs nanofluid is utilized as the coolant with varying concentrations. Cooling performance is investigated across discharge rates of 2c, 3c, and 4c, considering different coolant flow rates.

Table 5: Volumetric heat generation values for various discharge rate [12].

Discharge rate	Volumetric heat generation (W/m^3)
2C	19452
3C	42400
4C	74163

Table 5 illustrates the volumetric heat generation (Q) corresponding to various discharge rates. For the purposes of this investigation, the battery is operated at a discharge rate of 3C, resulting in a volumetric heat generation rate of 42,400 W/m^3. The heat transfer coefficient (h) for the outer surfaces is set at 5 W/(m^2 K). The ambient temperature (T_0) is fixed at 298.15 K. Inlet conditions are defined as a velocity inlet, and the outlet is configured as a pressure outlet with a gauge pressure of 0 Pa. Given that the Reynolds number is below 2300, the coolant flow is classified as a laminar flow regime. The resolution of the governing equations employs FLUENT 19.2, utilizing the Semi-Implicit Method for Pressure-Linked Equations (SIMPLE) approach as the solver [11].

2.2.2 Grid independence test and validation of method

The grid independence test was conducted over the BTMS1 using nf3 coolant at an inlet velocity of 0.12 m/s. The boundary conditions include 5 W/m^{2}K of heat dissipated from the surface of cells and 42000 W/m3 of heat generated in cells due to a 3C discharge rate. Since the flow is under a laminar regime, laminar flow is considered, and the Fluent 19.2 solver was used. The numerical equations are solved using the SIMPLE method. Cooling performance is checked at different numbers of grids. The maximum temperatures of the facets are 299.34K, 299.04K, 298.86K, and 298.85K, corresponding to grid numbers 99814, 148157, 646350, and 844320, respectively. The results remain almost constant after 646350 grids; hence, further analysis is based on this independent grid with 646350 grids. The meshing type used was a 3D tetragonal mesh. To validate the computational method, the same model as used by Wei Li et al. [12].

3. Results and discussion

Figure 3 shows the temperature distribution on the BTMS. This temperature distribution is with respect to a heat generation of 3c and a velocity of 0.12. The cooling of the cells in the 3rd row of BTMS1 is lower, but overall, there is uniform cooling. The reason for this uniformity is the high contact surface area, which has increased the heat transfer area, resulting in uniform cooling. If we consider BTMS3 and BTMS4, we can observe that their cooling performance is lower because of the lesser contact area to the cells, leading to reduced heat transfer from the cell to the nanofluid. Overall, the results indicate that temperature uniformity is better in BTMS1 and BTMS2 compared to BTMS3 and BTMS4.

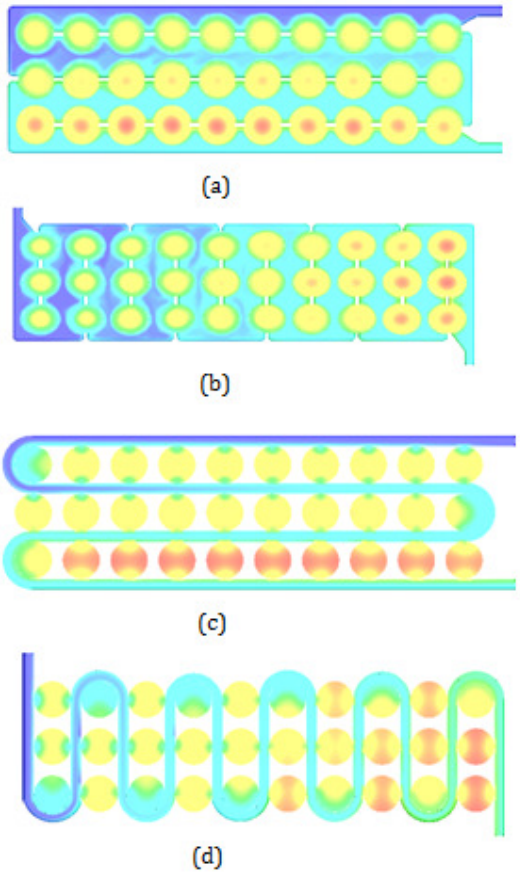

Figure 3: Contours of temperature variation in cooling channels at 3C discharging rate and 0.12 m/s inlet velocity of (a) BTMS1; (b) BTMS2; (C) BTMS3; (D) BTMS4.

Figure 4(a, b, c, d) illustrates the surface temperature of BTMS over time, corresponding to a volumetric heat generation of 3°C w/m³ and a velocity of 0.12 m/s. The graph depicts the cooling efficiency of BTMS using various nanofluids. In BTMS1 and BTMS2, the minimum surface temperature is associated with NF1 at 298.86 K and 298.87 K, while the maximum surface temperature of BTMS is observed at 299.05 K and 299.02 K with respect to NF4. It is noteworthy that there is a significant temperature difference among the nanofluids. Beyond 300 seconds of flow time in BTMS1 and BTMS2, the temperature becomes constant. This is attributed to the coolant absorbing all the heat generated by the lithium cell. In other words, the heat dissipated into the atmosphere and absorbed by the coolant equals the total heat generated by the cell. In BTMS3 and BTMS4, the minimum temperatures are observed with respect to NF2 at 299.74 K and 299.8 K, while the maximum temperatures are associated with NF3 at 299.9 K and 299.95 K. The results suggest that in BTMS3 and BTMS4, nanofluid performance is nearly identical, indicating minimal differences due to a smaller heat-absorbing surface. Furthermore, it is noted that the temperatures reach equilibrium after 400 seconds. In summary, the results indicate that for surfaces with larger contact areas to the cell, thermal conductivity is not as crucial. Despite NF2 having the highest thermal conductivity, NF1 demonstrates superior cooling performance. Conversely, for smaller contact surfaces, the thermal conductivity of the nanofluid becomes more important. Additionally, it is observed that larger contact surfaces achieve faster thermal stability compared to smaller contact areas with the lithium cell.

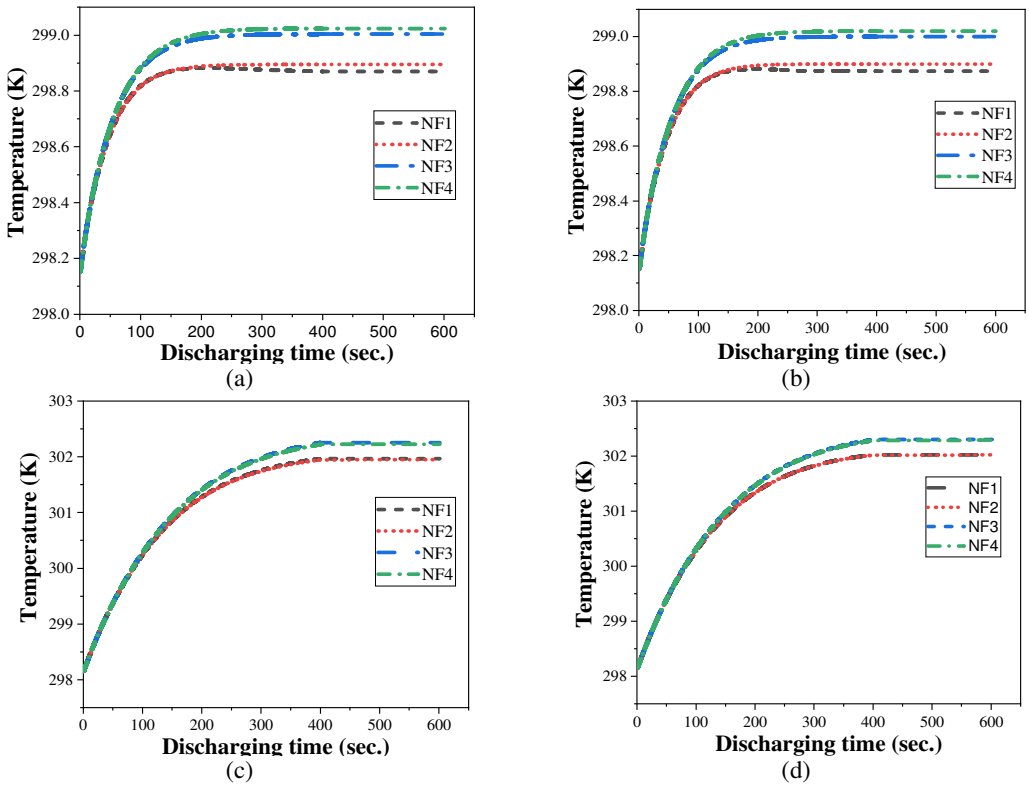

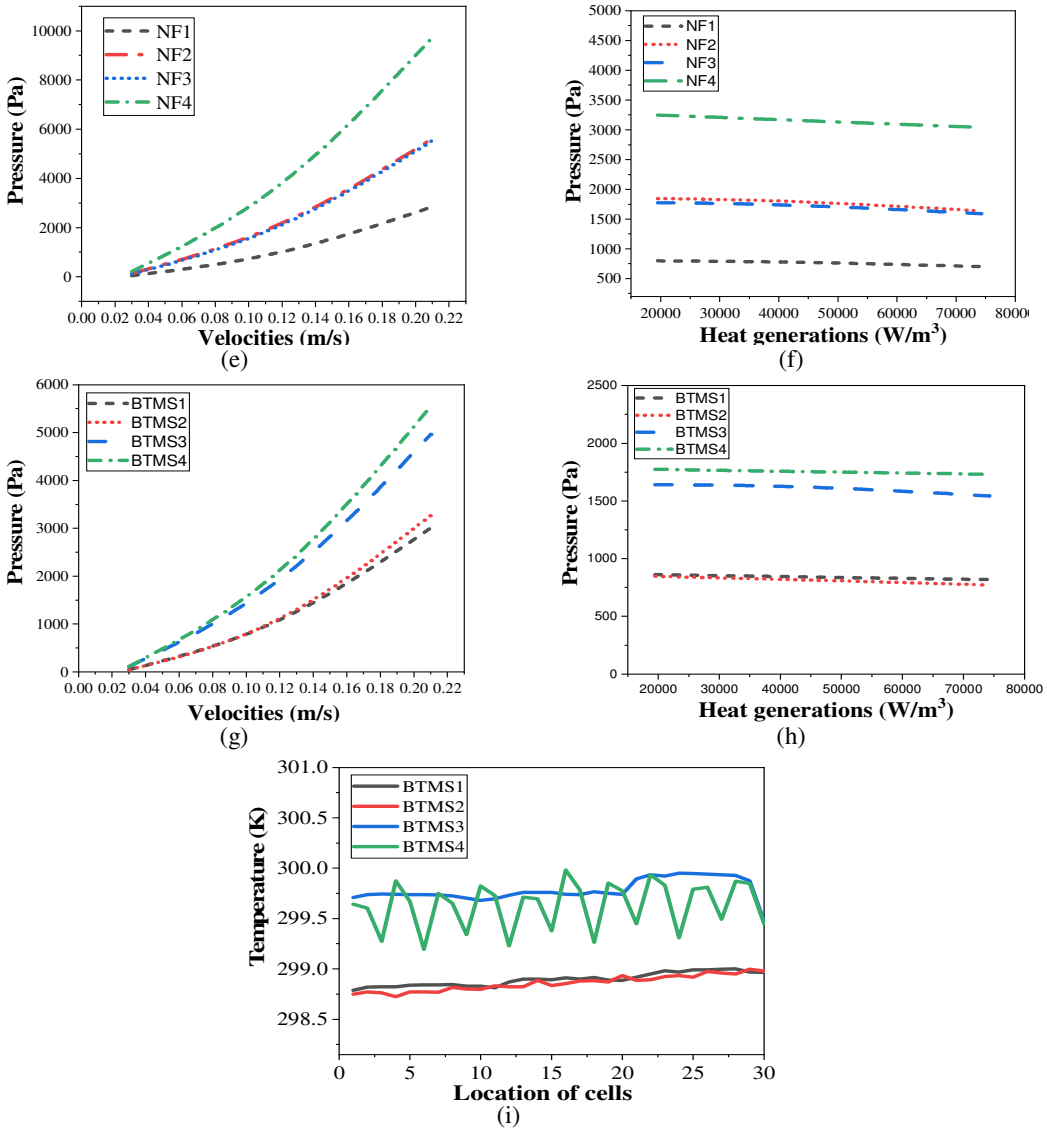

Figure 4: (a) BTMS1 (b) BTMS2 (c) BTMS3 (D) BTMS4 temperature variation at 3c discharging and velocity 0.12 m/s,(e) and (f) pressure variation at BTMS1 with respect to velocities and discharge rates, (g) and (h) pressure variation at NF1 in various BTMS respect to velocities and discharge rates.

Figure 4(e, f, g, h) illustrates the pumping power of BTMS across different velocities and discharge rates. In Figure 4(e), a graph depicts the relationship between pumping power and inlet velocity of BTMS1 nanofluid at a 3c discharge rate. The analysis reveals that the maximum pumping power occurs with nanofluid NF4, registering 3034.9 watts, while the minimum is observed with NF1 at 2049.8 watts, both corresponding to an inlet velocity of 0.21 m/s. The heightened pumping force in NF4 can be attributed to increased ethylene glycol (EG), resulting in higher viscosity and nanoparticle density in the coolant. The pumping power experiences a gradual increase up to 0.12 m/s, followed by a steeper ascent. The rise in inlet velocity leads to elevated pressure drop, consequently boosting pumping force. In Figure 4(f), a graph portrays the relationship between pumping force and discharge rate at 0.12 m/s inlet velocity for BTMS1. The graph indicates that increasing the discharge rate results in a decrease in pumping power. This reduction is attributed to decreased viscosity due to the elevated temperature of the coolant. Comparing pumping power among different BTMS, as shown in Figure 4(g), and Figure 4(h), it is observed that BTMS1 requires the least power, while BTMS4 demands the most. The diminished power requirement in BTMS1 can be attributed to a decrease in nanofluid viscosity caused by an increase in temperature. Additionally, the design of BTMS1 contributes to lower power consumption through an increased flow cross-sectional area and enhanced heat transfer due to a higher contact surface area with the cell. Conversely, BTMS4 exhibits higher pumping power due to its greater density and lower coolant temperature. The extensive band in the channel throughout BTMS4 also plays a role in its increased pumping power. Figure 4(h), illustrates a decrease in pumping power with an increase in discharge rate, with a notable decline in BTMS2 due to its larger surface contact area with the cell. .

Figure 4(i) illustrates the temperature fluctuations of BTMS following the flow of fluid through the channel. This temperature fluctuation is in relation to a 3°C volumetric heat generation and an inlet velocity of 0.12 m/s. It is evident that

BTMS1 and BTMS2 exhibit a smooth heat variation in their cells, whereas BTMS3 and BTMS4 display significant temperature variations along the channel. Consequently, BTMS1 and BTMS2 demonstrate better uniformity compared to BTMS3 and BTMS4. BTMS4, in particular, experiences the most substantial temperature variation in the direction of flow due to increased surface contact with the channel. Cells with more surface contact exhibit lower temperatures, benefiting from enhanced heat transfer into the cooling channel attributed to an increased surface area. Conversely, cells with less surface contact, primarily tangential, register higher temperatures due to reduced heat transfer into the cooling channel.

4. Conclusions

The proposed design is rooted in Newton's law of cooling, to enhance cooling performance; the design strategically increases the heat transfer area by wrapping channels around lithium-ion cells. The results indicate effective cooling and temperature uniformity. In this study, three-dimensional numerical simulations are employed to investigate liquid flow, focusing on the use of nanofluids within channels to enhance heat dissipation in systems experiencing high discharge rates. The pressure drop is contingent on factors such as the flow area, channel length, and fluid properties. BTMS4 experiences the highest pressure due to its restricted flow area and numerous channel bends, while the minimum pressure is observed in BTMS2. The maximum surface temperature of BTMS is influenced by the heat transfer area and coolant properties. The lowest surface temperature is recorded in BTMS1 in comparison to NF1, which contains 30% EG in distilled water with 0.05% MWCNTs particles, while the highest is observed in NF4, which consists of 30% EG in distilled water with 0.05% MWCNTs particles. Pumping power rises with an increase in the coolant flow rate and density. Coolants with higher specific weight require more pumping power, but this decreases with rising coolant temperature. The cell's surface temperature increases in the direction of coolant flow as the coolant absorbs heat from the cells. BTMS1 demonstrates more uniform cell temperatures due to its higher heat transfer area.

References

[1] H.A. Hasan, A.A. Hatem, L.A. Abd, A.M. Abed, K. Sopian, Numerical investigation of nanofluids comprising different metal oxide nanoparticles for cooling concentration photovoltaic thermal CPVT, *Clean. Eng. Technol*. (2022).

[2] Z. Esmaeili, M. Khoshvaght-Aliabadi, Thermal management and temperature uniformity enhancement of cylindrical lithium-ion battery pack based on liquid cooling equipped with twisted tapes, *J. Taiwan Inst. Chem. Eng*. **148** (2023) 104671.

[3] A. Hassan, S.Z. Ilyas, A. Jalil, Z. Ullah, Monetization of the environmental damage caused by fossil fuels, *Environ. Sci. Pollut. Res*. **28** (2021) 21204–21211.

[4] C. Zhao, A.C. Sousa, F. Jiang, Minimization of thermal non-uniformity in lithium-ion battery pack cooled by channeled liquid flow, *Int. J. Heat Mass Trans*. **129** (2019) 660-670.

[5] M. Kiani, S. Omiddezyani, E. Houshfar, S.R. Miremadi, M. Ashjaee, A.M. Nejad, Lithium-ion battery thermal management system with Al2O3/AgO/CuOnanofluids and phase change material, *Appl. Therm. Eng*. **180** (2020) 115840.

[6] P. Naphon, L. Nakharintr, S. Wiriyasart, Continuous nanofluids jet impingement heat transfer and flow in a micro-channel heat sink, *Int. J. Heat Mass Trans*. **126** (2018) 924-932.

[7] I. Mokashi, A. Afzal, S.A. Khan, N.A. Abdullah, M.H.B. Azami, R.D. Jilte, O.D. Samuel, Nusselt number analysis from a battery pack cooled by different fluids and multiple back-propagation modelling using feed-forward networks, *Int. J. Therm. Sci*. **161** (2021) 106738.

[8] P. Naphon, L. Nakharintr, S. Wiriyasart, Continuous nanofluids jet impingement heat transfer and flow in a micro-channel heat sink, *Int. J. Heat Mass Trans*. **126** (2018) 924-932.

[9] B. Abreu, Rheological characterization and modelling of CNT nanofluids, Universidade de Aveiro (Portugal) ProQuest Dissertations & Theses (2018).

[10] H.M. Maghrabie, K. Elsaid, E.T. Sayed, M.A. Abdelkareem, T. Wilberforce, M. Ramadan, Intensification of heat exchanger performance utilizing nanofluids, *Int. J. Thermofluids* **10** (2021) 100071.

[11] H. Versteeg, W. Malalasekera, *An Introduction to Computational Fluid Dynamics: The Finite Volume Method*, Pearson, Essex, UK (1995).

[12] W. Li, A. Garg, M. Xiao, L. Gao, Optimization for liquid cooling cylindrical battery thermal management system based on Gaussian process model, *J. Thermal Sci. Eng. Appl*. **13** (2021) 021015.

[13] W. Ajeeb, M.S. Oliveira, N. Martins, S.S. Murshed, Forced convection heat transfer of non-Newtonian MWCNTs nanofluids in microchannels under laminar flow, *Int. Commun. Heat Mass Trans*. **127** (2021) 105495.